JOURNAL OF SPACECRAFT AND ROCKETS
Vol. 46, No. 3, May–June 2009

Optimal Aft End Distorted Fin Model Using Response Surface Method

Se-Yoon Oh*
Agency for Defense Development, Daejeon 305-600, Republic of Korea
and
Seung O. Park†
Korea Advanced Institute of Science and Technology, Daejeon 305-701, Republic of Korea

DOI: 10.2514/1.40496

In wind-tunnel testing of bomb or missile-type models, aft end geometry distortion may become necessary when a model is tested by using a sting support system. When the diameter of the model base is increased, the exposed tail fin area is reduced to result in aerodynamic data alteration. In the present work, various tests are conducted on an MK-82 bomb model with base diameter and exposed tail fin area variations. The tests use techniques involving design of experiments and response surface modeling. The effects of the model base geometry modifications on the aerodynamic characteristics are investigated. Experimental design optimization is then performed on the basis of three design factors: the base diameter, the extended tail fin area, and the freestream velocity. The experimental results show that the altered aerodynamic characteristics due to aft end model distortion can be minimized by changing the tail fin geometry on the basis of the regression model.

Nomenclature

A	=	extended tail fin area ratio, S_t'/S_t
C_{m_α}	=	pitching moment coefficient slope
C_{N_α}	=	normal force coefficient slope
c_{tail}	=	tail volume coefficient
D	=	reference body diameter or maximum diameter
D_b	=	base diameter of the model
K_{b-t}	=	body–tail interaction factor
K_{w-b}	=	wing–body interaction factor
L_t	=	tail moment arm, $X_{\text{cg}} - X_{\text{cp}(t)}$
Re_D	=	Reynolds number based on the reference body diameter
S	=	missile reference area, $\pi D^2/4$
S_t	=	exposed tail fin area
S_w	=	exposed wing area
S_t'	=	extended S_t
U_r	=	95% confidence uncertainty
X_{cg}	=	center of gravity location from nose tip
$X_{\text{cp}(\,)}$	=	center of pressure location from nose tip
α	=	angle of attack, deg
ΔC_{m_α}	=	pitching moment coefficient slope change
ΔC_{N_α}	=	normal force coefficient slope change
ψ	=	angle of yaw, deg

I. Introduction

THIS study aims to find a way to minimize distortion effects on aerodynamic data due to the inevitable model distortion caused by sting support in wind-tunnel testing. Most missiles and stores are bodies of revolution, and their wind-tunnel test models are usually handled with sting mounts because the sting mount produces less aerodynamic interference than vertical support mounts, such as belly supports or blade struts. When a test model does not have a base area large enough for sting support due to restrictions of the wind tunnel, it may be necessary to modify the geometry of the model aft end. Usually the model base diameter is increased so that the effective surface area of the tail fin is reduced; however, this type of reduction means that the aerodynamic characteristics of the test model differ from those of an undistorted model.

The model aft end distortion corrections of aerodynamic data are quite different from the usual support interference corrections [1]. Nonsimilar geometric change in the aft end of the model makes the correction more difficult; and additional tests on an undistorted model are required for reference data. Although various works have focused on the sting interference correction of flow distortion, aerodynamic correction techniques for geometric model distortion are rare because most wind-tunnel tests assume geometric similarity between the model and the prototype. An example that convincingly demonstrates the need to study geometrically distorted model testing is the store model test of a captive trajectory system. The external shape modification may be compulsory due to the conflicting requirements of a scaled-down model (typically, 0.05-scale models are used) and the sting support [2,3]. Aerodynamic data that are modified as a result of model aft end distortion are likely to cause a substantial change in trajectory [2]; hence, if available, undistorted aerodynamic data should be used on account of the geometric distortion of the model.

To establish a reliable model modification and compensation process for the distortion effects, we first need to determine the effect of the tail fin design parameter on aerodynamic characteristics. In the present work, we considered three factors as design variables for the purpose of developing a compensation technique for the aft end distortion problem of a model of the MK-82 bomb. The three factors are the test velocity (V), the aft end distorted model base diameter (D_b), and the extended area ratio of the tail fins (A) based on the fin planform area. We chose the design of experiment-based response surface methodology (DOE/RSM) [4,5] to investigate the effects of the tail fin design. The DOE/RSM technique has been widely used in recent wind-tunnel experiments [6–14], and a number of studies that use the DOE/RSM technique for wind-tunnel tests have been published. DeLoach et al. [6–10,12] have made significant contributions in this regard.

The first part of this paper investigates the nature of the model aft end distortion problem and introduces the notion of the equivalent tail volume to deal with this undesirable contour alteration. The

Received 19 August 2008; revision received 18 November 2008; accepted for publication 23 December 2008.

*Senior Researcher, Wind Tunnel Test Division, Yuseong Post Office Box 35-12; also Ph.D. Student, Korea Advanced Institute of Science and Technology, Daejeon 305-701, Republic of Korea.

†Professor, Department of Aerospace Engineering, 373-1 Kusong-dong, Yuseong-gu. Senior Member AIAA.

Fig. 1 Distorted MK-82 model and undistorted model with image supports.

second part focuses on the DOE/RSM technique as a means of compensating for the distortion effects. Finally, there is a presentation of the experimental results for the various distorted tail fin designs based on the DOE/RSM technique.

II. Experimental Details

For many scaled-down experiments on unguided, nonpropelled bomb-type configurations, the diameter of the sting in the test model may be greater than the diameter required by the geometric similarity rule, especially if the sting has to withstand experimental conditions such as tunnel starting loads and maximum steady-state loads [15]. In these circumstances, the aft end shape of the model should be made large enough to accommodate the tail sting support, and this increase in size causes the aft end model to be distorted. The present work concerns the way the aerodynamic data is altered due to distorted aft end models of the 50% scale MK-82 bomb with fixed cruciform (x-type) tail fins at low subsonic speeds. As the main purpose of this work is to investigate the effects of aft end distortion, we simply selected nine different distortion cases (that is, three base diameters by three extended fin areas). Experiments were carried out in a low-speed wind tunnel to obtain aerodynamic data for various tail fin configurations. The tunnel is a solid-wall single-return closed-circuit tunnel with a 9:1 contraction. The test section has an area of 3×2.25 m and a length of 8.25 m. The average axial turbulence level of the tunnel is about 0.08%, and the nonuniformity of the tunnel flow angle is less than 0.1 deg. Aerodynamic forces and moments were measured with an internal six-component strain gauge balance at a sampling frequency of 10 Hz, and the data were averaged over 50 samples. An MC-10-1.50-A internal six-component strain gauge balance (manufactured by MicroCraft Technology, San Diego, California) was used. The load ranges of the balance are as follows: normal force up to 1000 lbf and pitching moment up to 2000 in. $\cdot$ lbf. The overall accuracy of the balance is within $\pm 0.1\%$ of the full scale.

Figure 1 illustrates a scaled-down MK-82 distorted fin model mounted on a crescent arc system with a rear sting support. A forced transition technique [15] was adopted to ensure a turbulent flow. Transition dots of 0.28 mm (0.011 in.) in height were attached to the nose at 5% of the body length position from the nose tip and on the tail fins at 15.7% of the chord from the leading edge. As shown in Fig. 2, the present MK-82 model has characteristics that are very common in missile and bomb designs, namely, a tapered afterbody and cruciform tail fins [16]. The tail fin has a tapered planform, as can be seen in Fig. 2.

Under geometric model discrepancies [2], the variation of the longitudinal static stability derivatives, such as the C_{N_α} and C_{m_α} values of a slender-finned bomb at subsonic Mach numbers, is much larger than the corresponding variation at supersonic Mach numbers. We therefore confine our attention to low subsonic flow cases. A simple equation for a normal force coefficient derivative of a missile-type body is given as follows [16], where the suffixes n, b, w, and t denote the contributions, from the nose, body, wing, and tail, respectively:

$$C_{N_\alpha} = (C_{N_\alpha})_n + (C_{N_\alpha})_w K_{w-b}(S_w/S) + (C_{N_\alpha})_t K_{b-t}(S_t/S) \quad (1)$$

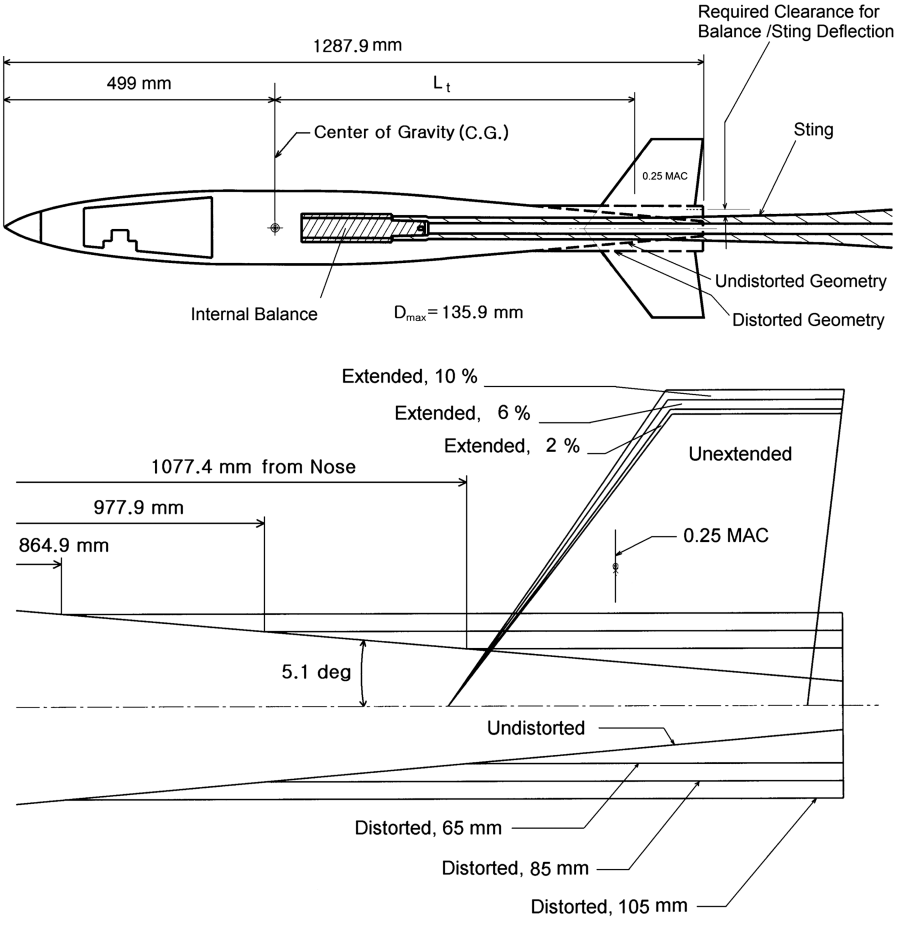

Fig. 2 Model configuration of the 50%-scale MK-82 model with extended tail fins and model bases.

Note here that the wing and tail area are the exposed areas; thus, in contrast to the planform area used in airplane aerodynamics, they do not include the area immersed in the body [16,17].

The pitching moment equation about the c.g. is expressed as follows [16]:

$$C_{m_\alpha} = (C_{N_\alpha})_n \frac{(X_{\text{cg}} - X_{\text{cp}(n)})}{D} + (C_{N_\alpha})_w K_{w-b}\left(\frac{(X_{\text{cg}} - X_{\text{cp}(w)})}{D}\frac{S_w}{S}\right) + (C_{N_\alpha})_t K_{b-t}\left(\frac{(X_{\text{cg}} - X_{\text{cp}(t)})}{D}\frac{S_t}{S}\right) \quad (2)$$

where various positions of center of pressure (X_{cp}) are dominant factors. We assumed that the location of the center of pressure of the tail was at 25% of the mean aerodynamic chord (0.25 MAC) of the tail fin.

The effectiveness of the tail in generating moment about the c.g. is proportional to the product of the normal force of the tail and the tail moment arm as given in Eq. (2). For this reason, the tail effectiveness is usually expressed by the tail volume coefficient as follows:

$$c_{\text{tail}} = \frac{\text{tail volume}}{\text{reference volume}} = \frac{(X_{\text{cg}} - X_{\text{cp}(t)})}{D}\frac{S_t}{S} = \frac{L_t}{D}\frac{S_t}{S} \quad (3)$$

Given the significance of the pitching moment in the dynamics of a missile or bomb-type body, the tail fin area should be changed (S_t') so that the tail volume coefficient remains unchanged. For simplification of the aft end distortion, it may be better to keep L_t (see Fig. 2) constant. For constant L_t, we need to change the tail fin geometry so that the location of 0.25 MAC of the tail fin does not change. Accordingly, both the aspect ratio (AR_t) and the sweepback angle (Λ_t) should be changed as shown in Fig. 2. With L_t constant, Eq. (3) tells us that we should change the tail fin geometry so that the exposed fin area remains the same as that of the (original) undistorted fin, thereby ensuring that the tail volume coefficient remains unchanged. However, this process is known to cause a significantly distorted C_{m_α}, partly due to the modifications of $(C_{N_\alpha})_t$ and K_{b-t} after the geometric distortion. Thus, an aerodynamicist must decide which fin area would be the best for minimizing the distortion in C_{m_α}.

Figure 3 presents pitching moment curves for various extended tail fin cases from our preliminary experiment. An independent wind-tunnel test was conducted to acquire data from an undistorted model (dashed line in Fig. 3) for reference. To evaluate and remove the strut support interference effects, we installed a dummy, or image, strut support that is identical to the original strut support shown in Fig. 1. The use of image support for the correction of the interference effect is well known [1,15]. For the distorted model tests, the rear sting interference effects were accounted for in terms of the flow angularity correction runs (upright and inverted runs) and the additional ΔC_m correction from the pitching moment coefficient difference in the upright and inverted runs [15]. The uncertainty estimates of various measurements of the present work were carried out in accordance with AIAA standard S-017A-1999 [18]. The uncertainties in the pitching moment coefficient for the undistorted model were found to lie between 0.0584 at $\alpha = 0$ deg and 0.0586 at $\alpha = 5$ deg. Figure 3 clearly illustrates the need to change the exposed tail fin area so that the effect of the aft end body distortion can be properly explained. We see that the case of a 2% area extension yields a pitching moment curve closest to that of the undistorted model. However, in an experiment based on the traditional one-factor-at-a-time approach, it is hard to determine the exact extended area required to correctly produce the pitching moment

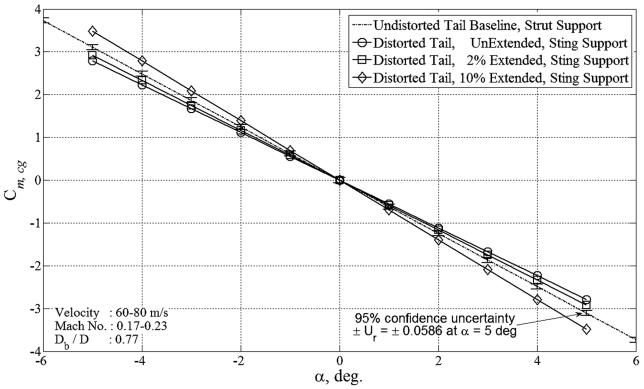

Fig. 3 Pitching moment curves for various MK-82 model aft end conditions.

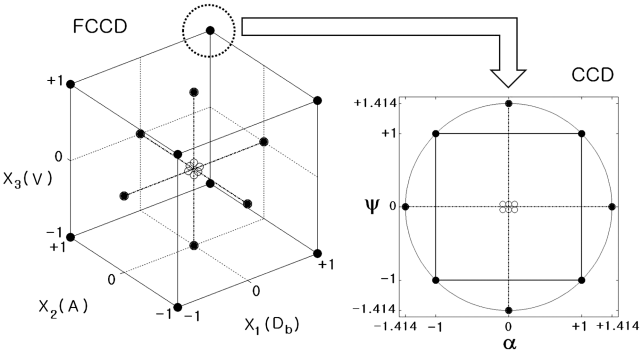

Fig. 4 FCCD and CCD for the DOE/RSM experiments (coded values).

curve of the undistorted model [4–14]. We therefore resorted to the DOE/RSM approach.

The central composite design (CCD) [4–7,9,10] is the most popular class of designs used for fitting a second-order regression model. In the present study, a DOE with a face-centered composite design (FCCD) [4,5,13,14] is applied to the RSM to determine how the tail fin design parameter affects the aerodynamic characteristics (Fig. 4). The experimental design variables in this work are the base diameter, the exposed tail fin area, and the test velocity. Three distorted model base diameters and three tail fin extended areas were selected to account for the effect of the aft end distortion. Three test velocities were chosen to examine the effect of the Reynolds number, even though the effect is not expected to be as significant as the normal force and the pitching moment is essentially independent of viscosity at low angles of attack. The independent circumscribed CCD experiments (Fig. 4) on the α and ψ combinations (with an α and ψ range from -5 to $+5$ deg, corresponding to ± 1 in the coded value) were conducted for various aft end distorted models. The three design factors with three levels are summarized in Table 1. In the FCCD test matrix, the factor of interest is denoted in the coded level (linear transformed level) given in Table 1.

The least-squares regression technique is usually applied to fit the RSM. This regression [4,5,7] is quite different from an ordinary regression because the regression in the DOE/RSM is a predefined–designed regression for a DOE approach. This DOE/RSM-based regression provides us with mathematical response models of longitudinal static stability derivatives as a function of all the design

Table 1 Factor levels for the FCCD experiments

Name	Factor	Units	Natural level (ξ_i) Low	Center	High	Coded level (x_i) Low	Center	High	Remark
Base diameter	D_b	mm	65	85	105	-1	0	$+1$	$0.48 \le D_b/D \le 0.77$
Extended fin area	A	%	2	6	10	-1	0	$+1$	$\Delta\Lambda_t = \pm 2.9°$, $\Delta AR_t = \pm 0.12$
Test velocity	V	m/s	40	60	80	-1	0	$+1$	$3.6 \times 10^5 \le \text{Re}_D \le 6.9 \times 10^5$

Table 2 FCCD matrix for experiments and measured results

STD No.	Run No.	D_b, mm	A, %	V, m/s	ΔC_{m_α}, 1/deg	ΔC_{N_α}, 1/deg
15	1	85	2	60	0.0091	0.0007
17	2	85	6	40	−0.0355	0.0112
13	3	65	6	60	−0.0569	0.0157
16	4	85	10	60	−0.0957	0.0240
20	5	85	6	60	−0.0443	0.0133
19	6	85	6	60	−0.0453	0.0142
14	7	105	6	60	−0.0161	0.0061
18	8	85	6	80	−0.0513	0.0145
6	9	85	6	60	−0.0454	0.0134
4	10	65	10	80	−0.1188	0.0307
3	11	105	2	80	0.0386	−0.0077
5	12	85	6	60	−0.0457	0.0138
1	13	65	2	40	−0.0006	0.0030
2	14	105	10	40	−0.0641	0.0174
11	15	85	6	60	−0.0465	0.0150
8	16	65	10	40	−0.1030	0.0272
7	17	105	2	40	0.0411	−0.0060
12	18	85	6	60	−0.0414	0.0122
1	19	105	10	80	−0.0757	0.0196
9	20	65	2	80	−0.0114	0.0063

factors in Table 1. The regression models used in the present study are of a second-order form as given in the following equation:

$$y = \beta_0 + \sum_{i=1}^{k} \beta_i x_i + \sum_{i=1}^{k} \beta_{ii} x_i^2 + \sum_{i=1}^{k-1} \sum_{j=2}^{k} \beta_{ij} x_i x_j + \varepsilon$$

$$\text{for } n \text{ observations} \quad \text{where } x_i = \frac{\xi_i - [\max(\xi_i) + \min(\xi_i)]/2}{[\max(\xi_i) - \min(\xi_i)]/2} \tag{4}$$

where each β is a model coefficient to be determined empirically; each x is a regressor; y is a response variable, such as the pitching moment coefficient; and ε is a normally and independently distributed random error or residual assumed to have a zero mean value and a constant variance. The variable x_i in Eq. (4) transforms the natural or actual variable ξ_i so that the value falls between −1 and +1 as in Table 1.

Table 3 Estimated uncertainties for a distorted model ($D_b = 85$ mm, $A = 6\%$, and $V = 60$ m/s)

Response	Test results with uncertainties	Name
C_A	$+0.1766 \pm 0.0509$	Axial force
C_Y	$+1.0356 \pm 0.1240$	Side force
C_N	$+1.0508 \pm 0.1462$	Normal force
C_l	$+0.0384 \pm 0.0394$	Rolling moment
C_m	-4.5371 ± 0.0639	Pitching moment
C_n	-3.9315 ± 0.0351	Yawing moment
α	$+6.1629$ deg ± 0.0348 deg	Angle of attack
ψ	$+4.9968$ deg ± 0.1119 deg	Angle of yaw

III. Results and Discussion

A. Experimental Data and Analysis

The parameters C_{m_α} and C_{N_α} of various aft end distorted models were obtained by varying α and ψ as specified in the CCD matrix of Fig. 4. These slopes for the distorted and undistorted models were obtained by using a least-squares fit for each data set (eight data points). The parameters ΔC_{m_α} and ΔC_{N_α} with respect to the undistorted model data were then calculated. The test results are summarized in Table 2. The uncertainties [18,19] in the aerodynamic force and moment coefficients for the distorted model are summarized in Table 3. The order of all the test runs was randomized to average out the influence of unknown variables over time. The tests were repeated six times about the center point ($D_b = 85$ mm, $A = 6\%$, and $V = 60$ m/s) of the FCCD matrix. Repeated runs of the same test achieved a repeatability value of $C_{m_\alpha} = \pm 0.00180/$ deg.

The Minitab [20] and the Design-Expert [21] software packages were used for data processing of the CCD matrix generation, regression analysis, analysis of variance (ANOVA), and response optimization. Table 4 gives regression analysis results of ΔC_{m_α} in coded units. The coefficients represent the mean change in response, ΔC_{m_α}, for one unit of change of the corresponding factor while holding other factors constant. The p value in the table for each regression coefficient tests the null hypothesis H_0 [4,5]. In general, a low p values suggests that the corresponding regressor variables (x_i) contribute significantly to the regression model. However, by comparing the t-for-H_0 values of D_b, A, and V at a 5% level of significance, we see that D_b and A are much more significant variables than V. We also find that the quadratic term D_b^2 is more important than the other quadratic terms and interaction terms, even though its effect on the regression model is not critical. The regression results given in Table 4 indicate that the response surface is

Table 4 Estimated regression coefficients for ΔC_{m_α} ($R^2 = 99.88\%$, $R^2(\text{pred}) = 99.33\%$, $R^2(\text{adj}) = 99.77\%$)

Term	Coefficient	Standard errors	t for H_0 coefficient = 0	P value	Significance ($P < 0.05$)
Constant	−0.044320	0.000690	−64.226	0.000	Significant
D_b	0.021450	0.000635	33.792	0.000	Significant
A	−0.053410	0.000635	−84.142	0.000	Significant
V	−0.005650	0.000635	−8.901	0.000	Significant
D_b^2	0.007150	0.001210	5.907	0.000	Significant
A^2	0.000350	0.001210	0.289	0.778	Not significant
V^2	0.000250	0.001210	0.207	0.841	Not significant
D_bA	−0.001213	0.000710	−1.709	0.118	Not significant
D_bV	0.001562	0.000710	2.202	0.052	Not significant
AV	−0.001763	0.000710	−2.483	0.032	Significant

approximately linear in D_b and A. The various R^2 values (coefficient of determination) imply that the present regression model fits the data extremely well. An ANOVA table (testing for a lack of fit) for ΔC_{m_α}, which is not presented here, also indicates that the regression model adequately describes the measured ΔC_{m_α} data. The regression analysis results of ΔC_{N_α} are similar in character to those of ΔC_{m_α}; thus, we omitted the data here.

To guarantee the validity of the regression model, we must always ensure that none of the regression assumptions [4,5] are violated. For this purpose, we checked the normality assumption by constructing a normal probability plot of the residuals; the results are shown in Fig. 5. We see from Fig. 5 that the residuals are scattered around a straight line, which implies that the normality assumption is satisfied at a 5% level of significance. We also confirmed that the present regression curves do not violate the constant variance assumption and that the residuals are not correlated with each other.

Figure 6 shows a response surface plot and a contour plot of ΔC_{m_α} as functions of D_b and A. In this figure, the ΔC_{m_α} data from the measurement (20 data points) are marked with circles. The dashed-line curve on the response surface of the figure is discussed in Sec. III.B. To check the adequacy of the response model, we tested an extra tail fin model ($D_b = 85$ mm and $A = 4\%$) as a confirmation experiment. The measured value was compared with the prediction value from the regression model. Using our response model, we find that the 95% prediction intervals for this confirmation point are $-0.0220 \leq \Delta C_{m_\alpha} \leq -0.0130$ and $0.0045 \leq \Delta C_{N_\alpha} \leq 0.0096$. The actual measurement yielded values of $\Delta C_{m_\alpha} = -0.0141$ and $\Delta C_{N_\alpha} = 0.0070$, which clearly demonstrates the accuracy of the present response model.

B. Response Optimization

This section concerns the question of how to select an extended fin area that minimizes the aerodynamic distortion when a specific (distorted) base diameter and velocity are given. The dashed line in Fig. 6, which is the curve of $\Delta C_{m_\alpha} = 0$ on the response surface, graphically illustrates the situation. When the base diameter is 84 mm, we find from the curve that the extended fin area should be 2.62% to give a zero-value ΔC_{m_α}. When there are multiple response functions, a more systematic approach is required. In terms of the response surface method, that means finding the best factor or factors that yield an optimum response in which the desirability function [4,5] is used. The desirability function, d_i, is an objective function that ranges from 0 outside of the validity limits to 1 at the goal point. We use a composite desirability function [4], namely, $d_{\text{comp}} = \{d_1 \times d_2 \times \cdots \times d_m\}^{1/m}$, which refers to the weighted geometric mean of the desirabilities of the individual responses, where m is the number of responses in the measure. In the present case, we set the composite desirability function as follows:

$$d_{\text{comp}} = \{d(\Delta C_{m_\alpha}) \times d(\Delta C_{N_\alpha})\}^{1/2} \tag{5}$$

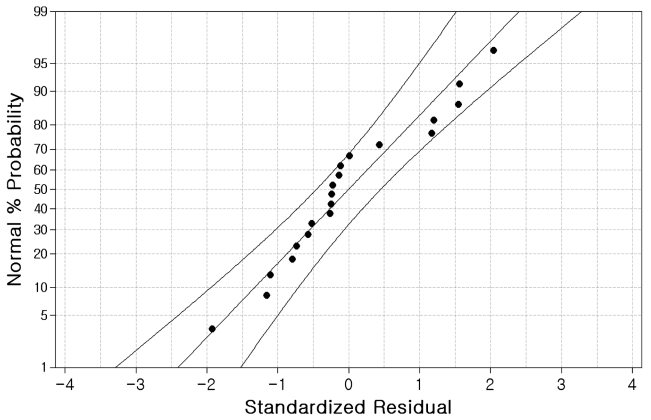

Fig. 5 Normal probability plot of residuals with a 95% confidence interval for ΔC_{m_α}.

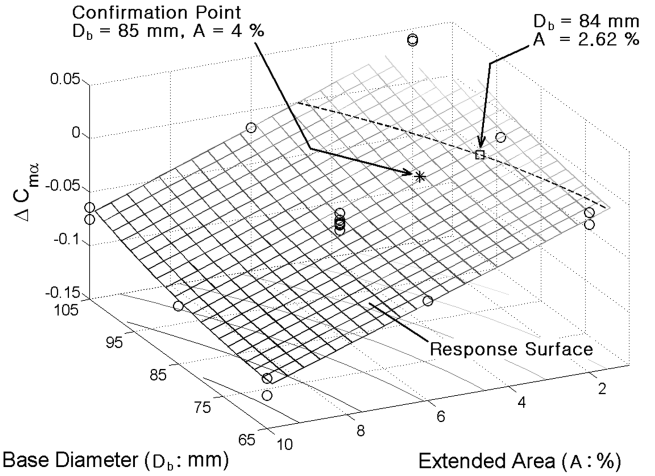

Fig. 6 Response surface and optimization solutions for ΔC_{m_α}; velocity at 60 m/s.

The design factors and object responses of the response optimization are listed in Table 5. For the purpose of presentation, we first set the test velocity to 60 m/s and the model base diameter to 84 mm as goal point values. We then search the optimum extended fin area that yields the maximum value of the desirability function. Obviously, the goal points for ΔC_{m_α} and ΔC_{N_α} are 0 whenever distortion-free conditions are desired.

Figure 7 shows the optimization plot. The vertical dashed-dotted lines on the graph and the numbers displayed at the top of each column represent the current design factor settings ($D_b = 84$ mm, $A = 2.62\%$, and $V = 60$ m/s). Various curves show how the desirability functions d_{comp}, ΔC_{m_α}, and ΔC_{N_α} vary with respect to the variable of each column whereas the other variables are kept constant at their optimum values. We again see that the extended fin area should be 2.62% when $D_b = 84$ mm and $V = 60$ m/s. In this case, the composite desirability, d_{comp}, becomes 0.95103 whenever ΔC_{N_α} is different from 0 with $d_2 \cong 0.905$.

An experimental aerodynamicist would be more interested in finding a suitable extended fin area when the base diameter has to be distorted by a certain amount. Figure 8 shows an overlay plot generated from the regression model for this purpose. The shaded area represents the range of the extended area that yields values of $\Delta C_{m_\alpha} = 0 \pm 1$ standard error in prediction ($\pm 1\sigma_{\text{SE}} = \pm 0.0020/$ deg in ΔC_{m_α} corresponding to $\pm 0.3\%$ of the pitching moment slope of the undistorted model). For example, we easily find that an extended fin area of 2% is needed when the base diameter is 75 mm. When the base diameter must be greater than that of the undistorted model, the tail fin area is inevitably immersed. From an aerodynamic viewpoint, we are interested in the amount of exposed fin area needed to properly compensate for the immersed area so that, in spite of this geometric distortion, C_{m_α} does not undergo any change. Figure 9 shows the relation between the extended area and the immersed area. When the base diameter is varied from 65 to 105 mm, the immersed area based on the fin planform is increased from 7 to 21% in the present case. Figure 9 shows that the extended fin area varies from 1.54 to 4.85% with an increase of the immersed area. We can easily see that the necessary extended area is approximately 24% of the immersed fin

Table 5 Parameters for response optimization

Factor (x)	Goal	Lower limit (L)	Upper limit (U)
D_b	Is equal to 84	65	105
A	Is in range	2	10
V	Is equal to 60	40	80
Response (y)			
ΔC_{m_α}	Is target (T) = 0	-	-
ΔC_{N_α}	Is target (T) = 0	-	-

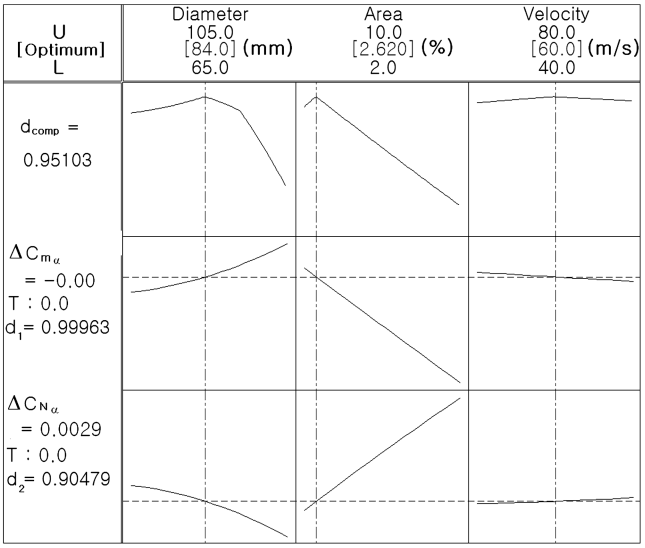

Fig. 7 Optimization plot for the response surface.

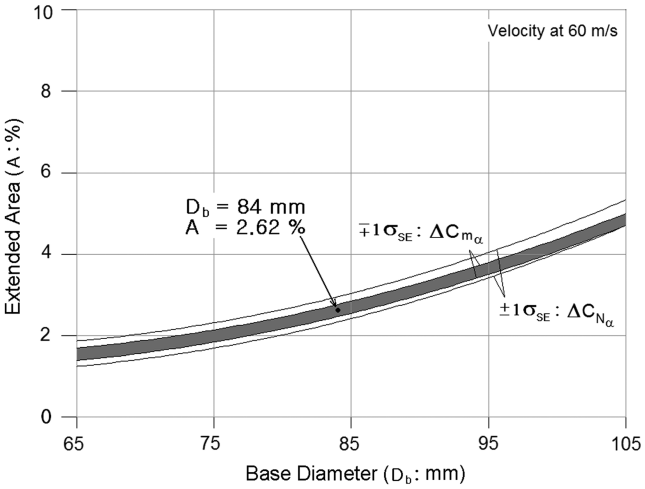

Fig. 8 Overlay plot for the response surfaces with a ±1 prediction standard error (σ_{SE}).

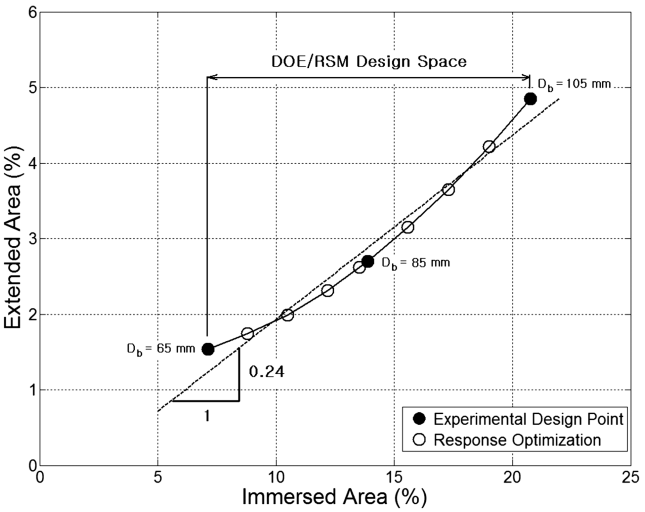

Fig. 9 Extended area vs immersed area; velocity at 60 m/s.

area. This result is consistent with the observation made in the computational study of [22] for the MK-84 (Joint Direct Attack Munition). This paper showed that, with a large sting, the area-matched fin configuration (that is, when the exposed fin area is simply increased by an amount corresponding to 100% of the immersed area) produced a very different pitching moment coefficient from that of the undistorted configuration.

IV. Conclusions

Low-speed wind-tunnel tests were conducted to clarify the aft end distortion effects on aerodynamic data for a model of an MK-82 bomb. To determine the relation between the increased base diameter and the extended tail fin area of a distorted model, we performed various tests based on DOE theory and processed data by using the RSM. A regression model was found to successfully determine the extended area of the tail fin needed to yield zero distortion effects on C_{m_α}. Our experimental data confirm that we need to increase the exposed tail fin area by only 24% of the tail fin area that is immersed due to the increased diameter of the base.

References

[1] Whitby, D. G., "Wind Tunnel Support System Effects on a Fighter Aircraft Model at Mach Numbers from 0.6 to 2.0," Arnold Engineering Development Center, AEDC-TR-89-4, July 1989.

[2] Carman, J. B., Jr., "Store Separation Testing Techniques at the Arnold Engineering Development Center, Volume I: An Overview," Arnold Engineering Development Center, AEDC-TR-79-1, Aug. 1980.

[3] Hill, D. W., Jr., "Investigation of Factors Affecting the Wind Tunnel Measurement of Carriage-Position Airloads on Experimental Store Models at Transonic Mach Numbers," Arnold Engineering Development Center, AEDC-TR-75-12, Feb. 1975.

[4] Montgomery, D. C., *Design and Analysis of Experiments*, 6th ed., Wiley, Hoboken, NJ, 2005, pp. 373–463.

[5] Myers, R. H., and Montgomery, D. C., *Response Surface Methodology: Process and Product Optimization Using Designed Experiments*, 1st ed., Wiley, New York, 1995, pp. 1–123, 208–265.

[6] DeLoach, R., "Application of Modern Experiment Design to Wind Tunnel Testing at NASA Langley Research Center," AIAA Paper 98-0713, Jan. 1998.

[7] DeLoach, R., "Tailoring Wind Tunnel Data Volume Requirements Through the Formal Design Of Experiments," AIAA Paper 98-2884, June 1998.

[8] DeLoach, R., "Improved Quality in Aerospace Testing Through the Modern Design Of Experiments," AIAA Paper 2000-0825, Jan. 2000.

[9] DeLoach, R., and Cler, D. L., "Fractional Factorial Experiment Design to Minimize Configuration Changes in Wind Tunnel Testing," AIAA Paper 2002-0746, Jan. 2002.

[10] DeLoach, R., "MDOE Perspectives on Wind Tunnel Testing Objectives," AIAA Paper 2002-2796, June 2002.

[11] Landman, D., Simpson, J., Hall, B., and Sumner, T., "Use of Designed Experiments in Wind Tunnel Testing of Performance Automobiles," Society of Automotive Engineers, Paper 2002-01-3313, Dec. 2002.

[12] DeLoach, R., "The Modern Design of Experiments for Configuration Aerodynamics: A Case Study," AIAA Paper 2006-0923, Jan. 2006.

[13] Landman, D., Simpson, J., Mariani, R., Oritz, F., and Britcher, C., "Hybrid Design for Aircraft Wind-Tunnel Testing Using Response Surface Methodologies," *Journal of Aircraft*, Vol. 44, No. 4, July–Aug. 2007, pp. 1214–1221. doi:10.2514/1.25914

[14] Landman, D., Simpson, J., Vicroy, D., and Parker, P., "Response Surface Methods for Efficient Complex Aircraft Configuration Aerodynamic Characterization," *Journal of Aircraft*, Vol. 44, No. 4, July–Aug. 2007, pp. 1189–1195. doi:10.2514/1.24810

[15] Barlow, J. B., Rae, W. H., Jr., and Pope, A., *Low-Speed Wind Tunnel Testing*, 3rd ed., Wiley, New York, 1999, pp. 234–327.

[16] Chin, S. S., *Missile Configuration Design*, McGraw–Hill, New York, 1961, pp. 17–63, 94–106.

[17] Nesline, F. W., Jr., and Nesline, M. L., "Wing Size Versus Radome Compensation in Aerodynamically Controlled Radar Homing Missile," AIAA Paper 1985-1869, Aug. 1985.

[18] Anon., *Assessment of Experimental Uncertainty with Application to Wind Tunnel Testing (S-017A-1999)*, AIAA Standard Series, AIAA, Reston, VA, 1999.

[19] Coleman, H. W., and Steele, W. G., Jr., *Experimentation and Uncertainty Analysis for Engineers*, Wiley, New York, 1999, pp. 16–43.
[20] Minitab, Statistical Software Package, Ver. 15.1.0.0, Minitab, Inc., State College, PA, 2006.
[21] Design-Expert, Statistical Software Package, Ver. 7.0.0, Stat-Ease, Inc., Minneapolis, MN, 2005.
[22] Donegan, T. L., Bangasser, C. T., and Fox, J. H., "Computational Study of Effects for the Joint Direct Attack Munition (JDAM)," AIAA Paper 1998-2799, June 1998.

M. Miller
Associate Editor